

LCMem: A Universal Model for Robust Image Memorization Detection

Mischa Dombrowski¹ Felix Nützel¹ Bernhard Kainz^{1,2}

¹Friedrich-Alexander-Universität Erlangen-Nürnberg ²Imperial College London

mischa.dombrowski@fau.de

Abstract

Recent advances in generative image modeling have achieved visual realism sufficient to deceive human experts, yet their potential for privacy preserving data sharing remains insufficiently understood. A central obstacle is the absence of reliable memorization detection mechanisms, limited quantitative evaluation, and poor generalization of existing privacy auditing methods across domains. To address this, we propose to view memorization detection as a unified problem at the intersection of re-identification and copy detection, whose complementary goals cover both identity consistency and augmentation-robust duplication, and introduce Latent Contrastive Memorization Network (LCMem), a cross-domain model evaluated jointly on both tasks. LCMem achieves this through a two-stage training strategy that first learns identity consistency before incorporating augmentation-robust copy detection. Across six benchmark datasets, LCMem achieves improvements of up to 16 percentage points on re-identification and 30 percentage points on copy detection, enabling substantially more reliable memorization detection at scale. Our results show that existing privacy filters provide limited performance and robustness, highlighting the need for stronger protection mechanisms. We show that LCMem sets a new standard for cross-domain privacy auditing, offering reliable and scalable memorization detection. Code and model is publicly available at <https://github.com/MischaD/LCMem>.

1. Introduction

Synthetic data sharing has emerged as a promising avenue to overcome long-standing barriers to data access and collaboration. Across domains, vast amounts of valuable image data remain locked behind institutional and proprietary walls, hindering reproducibility, scalability, and equitable progress in machine learning. In healthcare, the majority of medical images are confined to isolated databases and electronic health record systems, where privacy concerns and

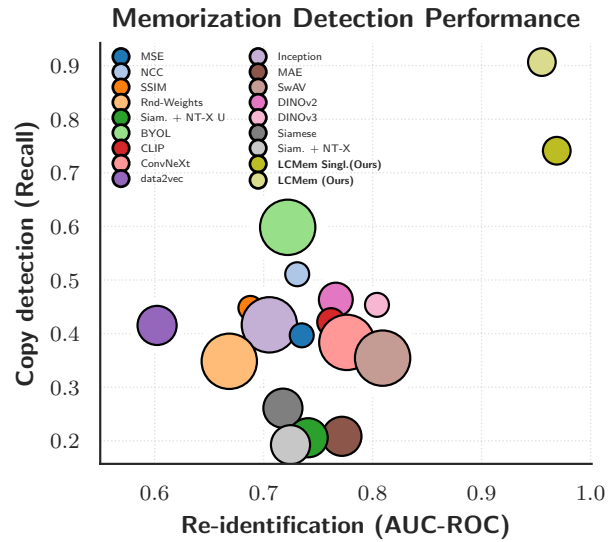


Figure 1. Joint performance of existing memorization detection methods across re-identification and copy detection. The visualization highlights the lack of models that perform well on both tasks simultaneously. Marker size denotes feature dimensionality.

regulatory constraints prevent data exchange across institutions [1, 47, 48, 56, 59, 69, 70]. Data silos limit the statistical power of medical studies and impede the development of robust, generalizable models. Legal frameworks such as the EU General Data Protection Regulation (GDPR) further restrict the processing of personal data, requiring that identifiability be excluded by “all means reasonably likely to be used” [13, 64]. Similar restrictions exist in the natural image domain. Copyright and data-ownership laws confine high-value datasets within proprietary repositories, often prohibiting redistribution or reuse for machine-learning purposes [6, 34, 42]. As a result, much of the world’s visual data cannot be freely shared, reproduced, or audited.

Two widely explored alternatives are federated learning, which enables collaborative model training without sharing raw data [19, 29, 44], and dataset distillation, which aims to

generate compact synthetic datasets that retain the information content of the original data [36, 68, 72]. However, both approaches face substantial practical limitations. Federated learning suffers from heterogeneous data distributions, regulatory restrictions, vulnerability to gradient inversion attacks, and the heavy coordination overhead required to synchronize distributed clients [5, 17, 19, 37, 75, 76]. Dataset distillation introduces statistical biases as rare cases are either omitted or disproportionately amplified.

In contrast, synthetic data generation provides a more direct and infrastructure-agnostic approach toward openly shareable, verifiably anonymized, and legally compliant datasets that preserve the statistical richness of the original data while respecting privacy, diversity, and intellectual property boundaries [13, 14, 55].

A central limitation of synthetic data sharing is the need for reliable mechanisms that guarantee the generated samples are truly synthetic and not memorized replicas of real images. The prevailing strategy is to train a model that predicts whether two images correspond to the same underlying instance, either through re-identification [52] or self-supervised similarity learning [12, 45, 55]. Yet these distance-based approaches rely on global dataset-level statistics, which leads to inconsistent behavior and overconfident decisions [33].

Existing memorization detection methods suffer from two central limitations: they are typically evaluated on a single dataset, leaving their cross-domain robustness unknown, and they treat re-identification and copy detection as separate problems. Re-identification determines whether two images depict the same instance, while copy detection tests whether an augmented image is still recognized as originating from the same source. For reliable privacy auditing, these tasks must be addressed jointly and evaluated across datasets and modalities, as their performance diverges markedly (see Fig. 1).

Our contributions are threefold. (i) We formalize memorization detection as a unified problem that integrates re-identification and copy detection. (ii) We demonstrate that existing models fail to solve both tasks simultaneously. (iii) We introduce LCMem, a large-scale memorization detector with a novel architecture and two stage training approach that operates in generative latent spaces and generalizes robustly across modalities and datasets.

2. Related Work

Image Generation: Diffusion models [24, 61] have emerged as the dominant paradigm for high-fidelity image synthesis, progressively transforming noise into structured data through learned denoising processes. Latent diffusion models (LDMs) [57] have improved scalability by operating in compressed latent spaces, enabling efficient large-scale training and commercialization. Instead of operating

in high-dimensional pixel space, LDMs make use of low-dimensional latent space representations. For an image resolution of $512 \times 512 \times 3$, this would usually result in a latent resolution of $64 \times 64 \times 4$. Recent advances further refined noise schedules, architectures, and guidance strategies to balance realism and diversity [23, 30–32]. However, despite their impressive fidelity, class-conditional and text-guided diffusion models remain prone to bias and limited distributional coverage [4, 14, 71]. To address these issues, diversity-aware diffusion models (DiADM) [14] decouple image quality from diversity, while PSO-secure generative models [13] extend this direction toward legally compliant, privacy-preserving synthesis, ensuring that no generated sample can be linked to a specific individual or record.

Memorization: Memorization has emerged as a critical vulnerability in generative modeling, as models can unintentionally reproduce training data with near-identical fidelity, revealing private or copyrighted content [8, 12]. Approaches to address this issue broadly divide into those that intervene during learning or sampling, and post-hoc filtering techniques applied after generation. The first group modifies the model’s optimization or sampling dynamics using mechanisms, like cross-attention regularization, data augmentation, or privacy-preserving objectives, to constrain overfitting [12, 54]. Differential privacy represents the strongest formal guarantee [74, 77], but is impractical for high-dimensional or high-resolution image synthesis, where utility degradation is severe and scalability limited. Post-hoc filtering, in contrast, does not alter model behavior but instead identifies and removes memorized outputs after sampling using re-identification, similarity search, or membership-inference based attacks [7, 8, 11, 13, 35, 52, 55]. This strategy has proven especially viable in large-scale diffusion pipelines, providing implicit privacy protection by detecting near-duplicates or direct copies of training images [12]. However, as shown by recent large-scale extraction studies [33], existing filters are still limited in specificity and consistency, often failing to detect reconstructive or partial memorization. Therefore, while post-hoc methods remain the most practical solution, advancing privacy assurance requires more robust methods and evaluation. We argue that one key limitation of existing approaches lies in the separation between copy detection, which yields more robust empirical predictions, and re-identification, which provides stronger formal guarantees. To address this gap, we perform extensive benchmarks across multiple datasets that jointly evaluate both paradigms, combining their complementary strengths in robustness and interpretability to achieve stronger and more verifiable privacy guarantees.

Applications of Synthetic Data: Synthetic data generation has proven effective for augmentation, dataset completion, imputation, and class balancing of real datasets [15, 41, 50, 65, 73]. Recent work shows that fully synthetic datasets

can closely match real-data performance [16, 21, 26, 27, 46, 55] even in privacy-secure generation frameworks stetings [13], yet a downstream performance gap remains.

3. Method

To train a unified memorization detection model, we begin with a collection of datasets that either include or do not include identity labels. These labels correspond to patient identity in medical datasets and may refer to a person, creator, or stylistic identifier in natural image datasets. We propose to leverage a pretrained autoencoder, identical to the one used by the generating diffusion model, to compute latent representations instead of working in image space. This allows us to precompute latents for all samples and train efficiently with large batch sizes. Given an image x , the autoencoder produces a latent $z = E(x)$ which can be used to get a nearly identical reconstruction $\tilde{x} = D(z)$. We employ the SDv2 autoencoder [57], which has been shown to preserve information necessary for downstream prediction tasks [13]. The reconstruction objective removes high-frequency noise that is irrelevant for identity matching, leading to quicker and more stable training of our model.

3.1. Memorization Detection Module

We train LCMem as a re-identification model. We show that a single model trained jointly for re-identification and copy detection performs worse, so we adopt a two-stage strategy. The first stage focuses on re-identification, and the second stage improves robustness and copy detection. The architecture is shown in Figure 2. The model receives two images and predicts whether they share the same identity label. A positive prediction indicates that both images belong to the same identity.

LCMem uses a Siamese backbone with a linear prediction head following [52]. We replace the earlier ResNet-based backbone with ConvNeXt-Tiny [40]. The model extracts features $u = S_\theta(z)$ and $u' = S_\theta(z')$ from latent tensors $z = E(x)$ and $z' = E(x')$. Since both branches operate separately, features for all real images can be stored and reused, which makes copy detection efficient. The prediction head receives the element-wise absolute difference $|u - u'|$ and outputs a probability that both samples belong to the same identity. Working in latent space reduces spatial resolution by a factor of 64. This drastically increases the model throughput and lowers the memory requirements, which enables large batch sizes and quick training on a single GPU. Furthermore, the latent space can be used as a much more condensed representation of the images themselves. The autoencoder is trained to ignore content that cannot be reconstructed such as noise, which is expected from the re-identification model anyway.

Before training, we compute and store all latent representations. Each dataset is normalized to zero mean and

0.5 standard deviation following [30]. A limitation of latent space training is that most image-space augmentations cannot be applied directly. To improve robustness for copy detection, the second stage fine-tunes the entire model on augmented image pairs, which are passed through the autoencoder before entering the Siamese backbone. Both stages also use a novel joint objective that combines re-identification and contrastive training. It combines the targets of the typical binary cross-entropy loss used for re-identification [52] and the contrastive NT-Xent loss used for copy detection in [10, 12],

$$\mathcal{L}_u = -\log \frac{\exp((u \cdot k_+)/\tau)}{\sum_{i=1}^K \exp((u \cdot k_i)/\tau)}. \quad (1)$$

where k_+ denotes all positive pairs across all pairs K in a batch and τ is a temperature hyperparameter fixed to 0.07.

The classification loss is

$$\mathcal{L}_{fc} = \text{BCE}(\text{MLP}(|u - u'|)). \quad (2)$$

The final training objective combines both losses as

$$\mathcal{L}_{\text{final}} = \alpha \mathcal{L}_u + (1 - \alpha) \mathcal{L}_{fc}. \quad (3)$$

Where α can be used to tune the influence of both losses. The contrastive term encourages features of matching identities to cluster together, while the classification term trains the predictor to decide whether two inputs correspond to the same identity.

Two-stage training: To achieve robustness, augmentations are essential. However, introducing them during early training destabilizes identity learning. We therefore train LCMem in two stages. Stage one trains on clean latent pairs using the combined loss function. During this first stage, the model can focus on the hard task of re-identification without perturbations that make the detection harder. The second stage applies strong augmentation to improve robustness and copy detection results. However, many augmentations cannot be straightforwardly applied to the latent space of the diffusion model due to the autoregressive nature of the autoencoder. Therefore, during the second stage the model applies the augmentation in image space and encodes the augmented image into latent space.

3.2. Applying Memorization Detection

The privacy model P corresponds to the trained LCMem classifier that predicts whether two inputs share the same identity. Unlike distance-based memorization detection methods [12, 55], our approach leverages explicit train-synthetic pairs, following the paradigm introduced by [13]. Each training sample is treated as its own class by computing a unique pseudoconditional label $c_s = f(c_r)$ from the real class label and a feature extractor f , such as the Inception-v3 network used for FID. A class-conditional

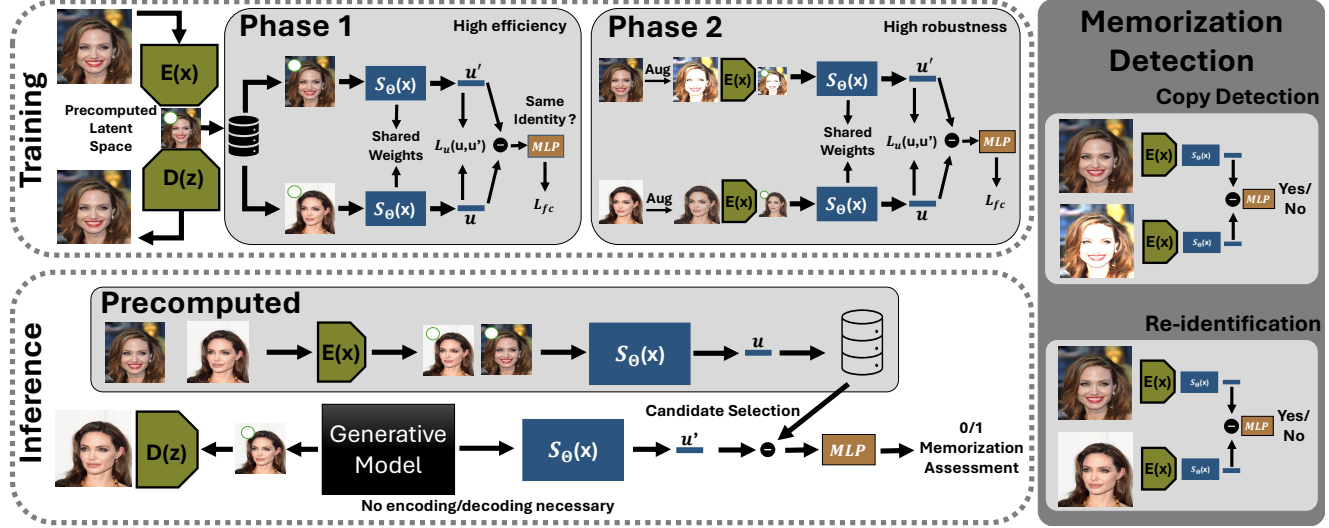


Figure 2. (Left) Training and inference workflow of LCMem. Latent images produced by the pretrained autoencoder are indicated with a green circle. (Right) Complementary structure of copy detection and re-identification in our unified framework.

diffusion model s is then trained to generate an image $x_s = s(c_s)$ from c_s . At sampling time, we apply post-hoc filtering by comparing each generated image to its corresponding training image and marking it as novel when $P(x_r, x_s) < 0.5$ for $x_s = s(f(x_r))$. If the model produces a sample that matches its training counterpart too closely, the sample is rejected and regenerated. Since P was trained in the latent space of the image generation model, we can directly apply it to the synthetic latent z_s produced by the image generation model without decoding it to image space. Furthermore, since the dataset of real images does not change, we precompute an atlas of real privacy vectors u_r .

4. Experiments

Datasets: The selection of the datasets was conducted with the goal of combining medical and non-medical datasets, and we focused on datasets with identity labels present to enable training of the re-identification module. Re-identification results are only computed for datasets where this label is present. We specifically focus on long-tail datasets because we believe that conditional image generation is especially useful in this setting. An overview of all datasets used is shown in Tab. 1. For a more balanced training, we oversampled smaller datasets.

Metrics: We report AUC-ROC and specificity for memorization detection in the re-identification setting. To do so, we exhaustively sample all positive pairings in the test dataset and then add one negative pairing by combining different images from the same dataset. To reliably measure memorization, we prioritize avoiding false negatives, since missed matches correspond to undetected memorized sam-

ples. We therefore define a strict false negative budget that limits how many such errors are acceptable. Because re-identification is a particularly difficult task, the remaining false negatives after applying this budget are the hardest cases to detect. Under this constraint, the model is allowed to filter only a small number of images. Consequently, for our re-identification benchmark, we fix the false negative rate at 1% and evaluate *precision at 99% recall*.

For evaluating copy detection, we first fit all methods to a threshold that achieves 95% recall on the validation set. We then randomly sample 1000 test images and apply a range of augmentations with increasing strength to measure copy robustness. Note that enforcing a higher recall threshold leads to less meaningful results for baseline methods due to their inherently low sensitivity.

Image Generation: To test our privacy model on generated data we train a pseudo-conditional diffusion model based on [14]. We report FID for generative quality and image-retrieval score (IRS) for generative diversity [14]. We use the output probabilities of a pretrained classifier $C(x_r)$ trained on each dataset individually to compute the pseudo-conditional labels c_s . The memorization rate is computed as the proportion of pairs (x_s, x_r) classified as identical by the privacy model P . Formally, for each real image $x_r \in D_r$, we define its corresponding pseudo-conditional feature as $c_s = C_r(x_r)$ and generate the synthetic counterpart $x_s = s(c_s)$. The privacy model then evaluates $P(x_s, x_r)$ which measures the similarity between the generated sample x_s and its corresponding real image x_r . A memorization event is counted when $P(x_s, x_r)$ outputs a positive prediction. The overall memorization rate is therefore given by

Table 1. Overview of the datasets used in our experiments. Datasets differ in whether they contain identity labels or not. If an identity label is present, copy detection corresponds to re-identification. If no identity label is available, the dataset is evaluated only on copy detection.

Dataset Name	Medical	Identity Label	# Images	Prediction Type	#(Labels/Classes)
CelebA [38]	\times	✓	202,599	Labels	40 facial attributes
ImageNet-LT [39]	\times	\times	185,846	Classes	1000 classes
MIMIC-CXR [28]	✓	✓	119,534	Labels	20 thoracic diseases classes
NIH-CXR-LT [25, 66]	✓	✓	84,158	Classes	20 thoracic diseases classes
ISIC-2020 [58]	✓	✓	32,701	Classes	Benign/Malignant classification
CTRate [20]	✓	✓	27,683	Labels	15 pulmonary disease labels

$$\text{MemRate} = \frac{1}{|D_r|} \sum_{x_r \in D_r} [P(s(C(x_r)), x_r) > 0.5]. \quad (4)$$

Benchmark Models To assess the performance of our model we compare it with a set of widely used foundation models and task-specific memorization detection models. This includes naive similarity metrics such as mean absolute error or SSIM [67], as well as foundation-model-based methods following the selection of [14, 62], extended with DINOv3 [60]. This list includes BYOL [18], CLIP [53], ConvNeXT [40], data2vec [2], DINOv2 [51], Inception [63], MAE [22], and SwAV [9]. For comparison, we also include a “Random” baseline that employs an untrained Inception-v3 [63], which has nevertheless been shown to provide useful feature representations [49]. For DINOv3 [60] we only consider output of the pooling layer of the smallest model because computational demands of larger models make its use infeasible for many low- to mid-resource tasks such as online evaluation of memorization. Preliminary results on smaller subsets showed no difference between the larger and the smaller models. For training the benchmark methods [12, 52], we used a ResNet-101 backbone with 512 and 1024 output features. Among these, we selected the best performing run. They were trained using their suggested parameters based on the respective publications. We compared [12], which is originally trained without identity labels, with a version that does use them.

Training details The first stage of the model is trained for 100 epochs or until convergence, with early stopping applied after 10 epochs of no improvement. At training time, positive pairs are sampled from images of the same identity, while negative pairs are drawn from different identities within the combined dataset. When identity labels are unavailable, the model operates in an unsupervised mode, in which positives are formed by applying privacy-preserving augmentations to the same image. Afterwards, the second stage, which additionally applies heavy augmentation, runs for 20 more epochs or five epochs of no improvement.

4.1. Re-Identification Model

The problem with current methods, as well as methods based on pre-trained foundation models, is also shown in Tab. 2. None of them perform consistently well across all datasets. When trained on multiple datasets simultaneously, their performance degrades sharply, suggesting that they do not form a meaningful representational space but instead collapse into task-specific re-identification cues that fail to generalize. Consequently, enforcing a strong threshold that filters out re-identifiable images would mean that specificity drops to less than 10% for all methods. Practically, this would mean that if we want to enforce a strong privacy filter, it would also remove many truly novel generations. This would lead to unnecessary rejection sampling burden due to filtering out too many false positives. We argue that the core issue is the inability of existing methods to learn a unified privacy model across datasets, despite their well established performance when trained on each dataset individually. Our method on the other hand maintains strong performance across all datasets with a single unified model, and its sensitivity remains high enough that even under large privacy budgets the filter preserves the vast majority of images. Contrary to our expectations, the two-stage training setup yielded slightly lower performance, suggesting that stronger image augmentations do not provide additional benefit for the re-identification objective in this setting.

4.2. Copy Detection

Next, we take the same models and benchmark them on the task of copy detection. For setting up a fair comparison, we calibrate the decision threshold for all methods to reach 50% specificity on the validation set for each dataset separately. Note that typically LCMem would not need this as it is automatically calibrated by being trained on binary classification. Then, we randomly sample 1000 positive test pairs to evaluate copy detection. We assess robustness by applying diverse augmentations at varying strengths and report sensitivity, defined as the point at which the model begins to judge the augmented sample as differing from its ground truth counterpart. Examples are shown in Fig. 3. For com-

Table 2. **Re-identification** benchmark across datasets. Each dataset is evaluated using AUC and specificity at a fixed sensitivity of 0.99. This reflects how many truly negative pairs are removed under strict sensitivity requirements. All task-specific models were trained jointly on the full set of datasets.

Method	CelebA		MIMIC-CXR		NIH-CXR-LT		ISIC-2020		CT-RATE		Macro Avg.	
	AUC	Specificity										
<i>Pixel-wise</i>												
MSE	0.579	0.013	0.661	0.015	0.765	0.049	0.747	0.029	0.922	0.210	0.735	0.063
NCC	0.598	0.018	0.672	0.017	0.733	0.021	0.747	0.046	0.904	0.005	0.731	0.021
SSIM	0.581	0.016	0.620	0.012	0.682	0.024	0.601	0.006	0.955	0.241	0.688	0.060
<i>Unsupervised</i>												
Random [49]	0.568	0.026	0.572	0.022	0.579	0.023	0.740	0.035	0.883	0.274	0.668	0.076
Siamese + NT-Xent [12]	0.558	0.017	0.806	0.062	0.808	0.062	0.717	0.041	0.816	0.147	0.741	0.066
<i>Foundation Models</i>												
BYOL [18]	0.601	0.016	0.721	0.007	0.767	0.047	0.661	0.045	0.859	0.190	0.722	0.061
CLIP [53]	0.956	0.539	0.635	0.015	0.695	0.029	0.736	0.041	0.787	0.103	0.762	0.145
ConvNeXt [40]	0.880	0.196	0.730	0.022	0.707	0.028	0.749	0.019	0.816	0.095	0.776	0.072
data2vec [2]	0.537	0.013	0.587	0.018	0.615	0.014	0.542	0.010	0.729	0.026	0.602	0.016
Inception [63]	0.693	0.058	0.676	0.027	0.706	0.036	0.633	0.030	0.818	0.091	0.705	0.048
MAE [22]	0.616	0.021	0.741	0.020	0.776	0.067	0.809	0.041	0.917	0.211	0.772	0.072
SwAV [9]	0.763	0.067	0.792	0.031	0.827	0.035	0.781	0.068	0.882	0.169	0.809	0.074
DINOv2 [51]	0.806	0.117	0.728	0.018	0.756	0.033	0.712	0.017	0.830	0.090	0.766	0.055
DINOv3 [60]	0.826	0.170	0.819	0.038	0.828	0.073	0.769	0.025	0.778	0.090	0.804	0.079
<i>Task-specific</i>												
Siamese [52]	0.550	0.017	0.712	0.010	0.799	0.051	0.647	0.009	0.880	0.240	0.718	0.065
Siamese + NT-Xent [12]	0.563	0.018	0.779	0.039	0.779	<u>0.089</u>	0.727	0.052	0.776	0.161	0.725	0.072
LCMem Single Stage (Ours)	0.950	0.625	0.994	0.891	0.997	0.946	0.933	0.697	0.972	0.512	0.969	0.734
LCMem (Ours)	0.955	0.645	0.996	0.933	0.997	0.951	0.916	0.570	0.914	0.167	0.955	0.653

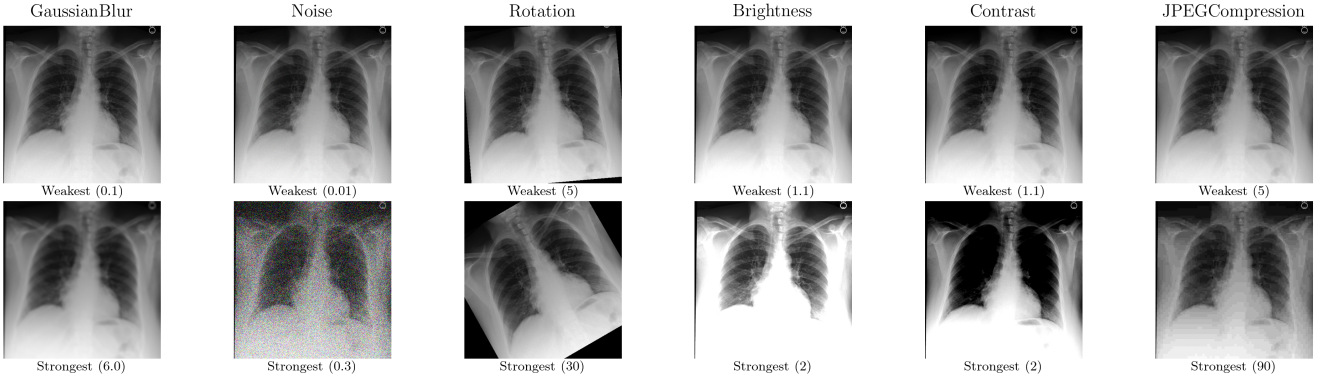


Figure 3. Example augmentation for copy detection. To evaluate model performance, we apply augmentations at varying strengths to each image (weakest and strongest shown) and test whether the model continues to recognize the augmented sample as a copy of the original.

parison we macro-average the recall on the strongest augmentation over all datasets and show it in Sec. 4.1. The results indicate superior copy detection performance of our method over all benchmark methods. Specifically, it shows that other task-specific models quickly drop in performance when being assessed for their robustness. For our models, we can see that without the second stage training, the model performance drops drastically. Importantly, this robustness will be crucial if generated images are simply augmentations of the training images. Across all benchmark methods, BYOL performed best, providing a robust argument for strong augmentations at training time for copy detection.

However, its performance on re-identification remains limited and would not provide sufficient privacy guarantees.

In Fig. 5 we show all augmentations applied for the copy benchmark. Across all augmentations, our model is most affected by extreme brightness changes, a setting in which BYOL attains the highest score at the strongest augmentation level. For all other augmentation techniques, LCMem outperforms all methods and shows strong robustness. Importantly, the results are stable across all tested noise strengths, where the single stage model collapsed. This may be particularly valuable for image generation scenarios where residual noise persists.

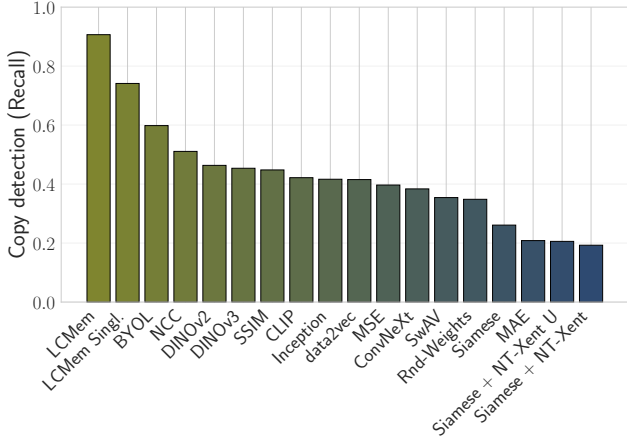


Figure 4. Copy detection performance across all datasets. Recall is reported at the strongest perturbation level and macro averaged. All models were calibrated to achieve 50 percent specificity.

Table 3. Generative performance and memorization detection for image generation using different conditioning strategies.

Conditioning	FID ↓	IRS ↑	Mem-Rate (%) ↓
Label + Noise	9.43	0.362	4.31
Prediction (Pred)	8.23	0.423	6.68
Pred + Label	7.25	0.479	6.32
Ensemble	9.68	0.479	7.04
Ensemble + Label	8.28	0.505	6.17

4.3. Applying Memorization Detection

To show an application of our LCMem in practice, we evaluate the memorization rate across five different conditioning methods. We consider different conditioning strategies derived from classifier predictions. Specifically, we use the sigmoid-activated outputs $p^{(k)} = \sigma(C_r^{(k)}(x))$ of classifiers $C_r^{(k)}(c|x)$ trained on the real dataset D in a five-fold setup. We compare using a single classifier prediction versus using the ensemble mean of the five classifiers. In addition, we examine whether explicitly including the ground-truth label c_r in the conditioning vector improves performance. We also include a baseline that replaces the classifier output with a randomly perturbed label $c_r + \epsilon$, where $\epsilon \sim \mathcal{N}(0, \sigma^2)$ is sampled once per sample and kept fixed. Across all metrics, incorporating label consistently improves performance. The combination of a single classifier prediction $p^{(k)}$ and the corresponding label c_r achieves the highest image quality, while the ensemble-based approach provides the greatest diversity. The results in Tab. 3 show that memorization rates remain consistently low across all methods and match the expected values given the filter’s false positive rate. Notable differences across runs nevertheless persist, for example when using an ensemble to generate pseudo-conditionals

for all methods.

4.4. One-vs-All Privacy Assessment

We apply LCMem in a one-versus-all setup, simulating the scenario in which a single generated image is compared against the entire training dataset. For MIMIC-CXR, we evaluate 16,125 test images from 5,125 patients, yielding 86,626 positive and 218,613,304 negative pairs. Exhaustive privacy scoring across all pairs completes in under seven minutes on a single GPU. For visualization, we randomly sample 10,000 predictions of each type, shown in Fig. 6. The distributions exhibit minimal overlap, consistent with the high AUC-ROC values in Tab. 2. Only a small number of positive pairs fall near the negative range, yet they remain above nearly all negative scores. This enables practical full-dataset privacy evaluation. Given a real test image x_a , all images x with different identities should produce negative predictions. If the generative model produced an unseen yet realistic image $x_s = x_a$, the filter would not reject it even under an exhaustive comparison. In practice, we observe this failure only once among 16,125 samples, indicating that while such cases are possible, achieving complete protection will require further improvements in privacy filtering performance.

4.5. Ablation Study

To substantiate our proposed changes to memorization detection training, we provide ablation results in Tab. 4. Results are micro-averaged over the whole training dataset. They show that applying augmentations during single stage training, even mild ones, consistently degrades performance. With a two stage setup, recall on positive pairs increases, although this comes at the cost of reduced precision. Additionally, Tab. 4 supports our combined loss function and the use of a pretrained autoencoder.

4.6. Computation Requirements

Latent representations are precomputed once per dataset, taking about one GPU hour for $N = 100,000$ samples. Training the privacy model uses a single Nvidia GH200 GPU. One epoch on all datasets in the first training phase takes two minutes. In the second stage, where image space augmentations are required and precomputing the dataset is infeasible, a single epoch takes about one hour.

4.7. Limitations

While our proposed LCMem effectively mitigates memorization, it does not prevent all potential risks such as membership inference attacks [74]. However, these attacks require access to both the model and the training data, which we assume to be unavailable to an adversary. Post-hoc filtering based on learned black-box detectors may lack interpretability, consistency and guarantees. For real-world use

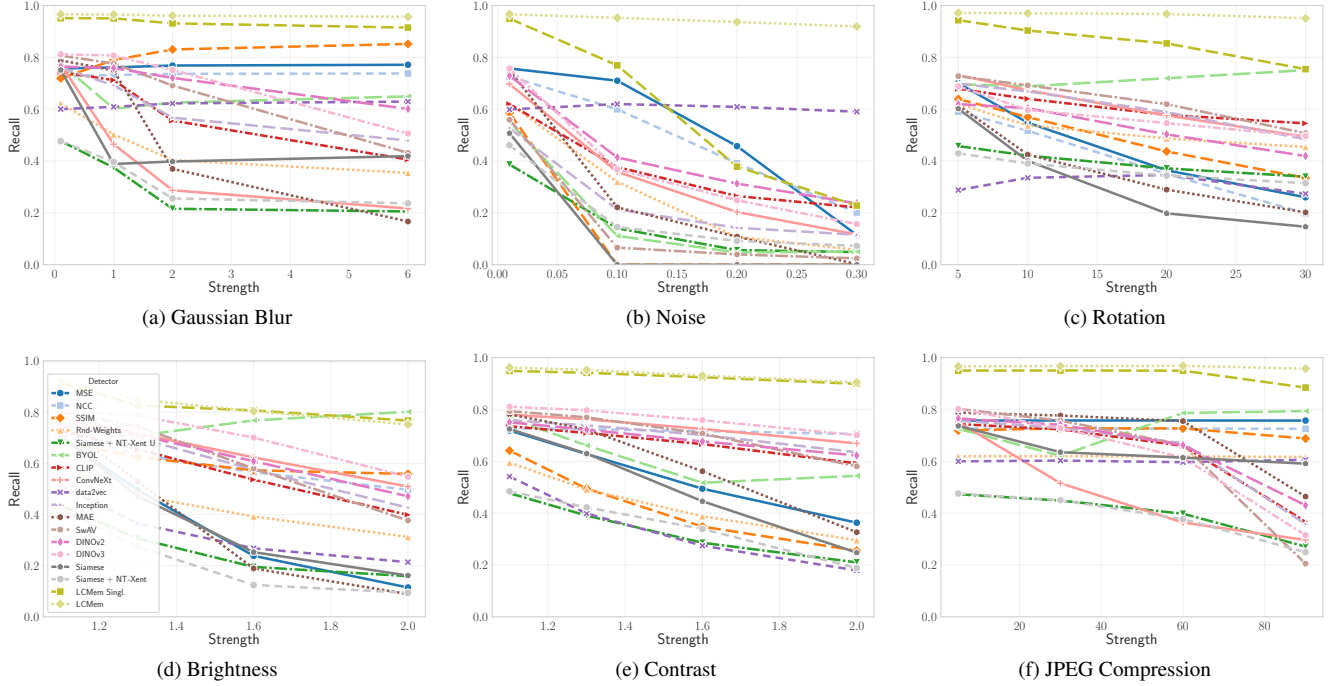


Figure 5. Per-transform recall vs. strength for six transformations. Thresholds were chosen based on achieving 50% specificity on the validation set. For ImageNet-LT, the models use the average thresholds over all other runs. Results were macro averaged over all datasets.

Table 4. Re-identification ablation experiments. Micro-average results given over all datasets. SWN refers to sample-wise-normalization. The numbers in augmentation refer to the different stages.

Backbone	Augmentation	α	Latent	Accuracy	F1-Score	Precision	Recall	AUC
ResNet-101	–	1	No	0.5973	0.6521	0.5749	0.7546	0.6409
ResNet-101	–	1	Yes	0.6692	0.7487	0.6036	0.9857	0.8100
ConvNeXt-Tiny	–	1	Yes	0.7102	0.7734	0.6349	0.9893	0.8622
ConvNeXt-Tiny	Rotate, Flip, Blur, Noise, SWN	1	Yes	0.7068	0.7702	0.6332	0.9831	0.8295
ConvNeXt-Tiny	Blur, Noise, SWN	1	Yes	0.6957	0.7645	0.6236	0.9878	0.8329
ConvNeXt-Tiny	Noise	1	Yes	0.6810	0.7567	0.6116	0.9920	0.8564
ConvNeXt-Tiny	–	0.8	Yes	0.8193	0.8444	0.7414	0.9808	0.9403
ConvNeXt-Tiny	–	0.5	Yes	0.8559	0.8708	0.7894	0.9709	0.9468
ConvNeXt-Tiny	SWN	0.8	Yes	0.8446	0.8633	0.7706	0.9813	0.9509
ConvNeXt-Tiny	(1) SWN (2) Rotate, Flip, Blur, Noise, Brightness, Contrast, JPEG	0.8	Yes	0.8324	0.8551	0.7531	0.9889	0.9555

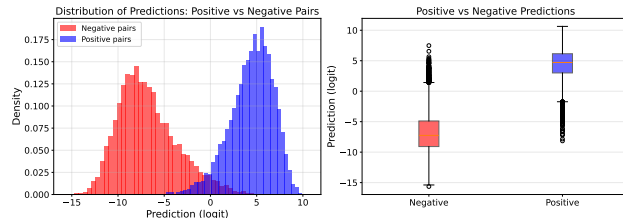


Figure 6. Exhaustive privacy prediction results on the full MIMIC-CXR test set. Limited to 10,000 samples for visualization.

cases, formal verification will be necessary. Moreover, reliable privacy auditing still requires dataset-specific training and careful empirical validation before deployment, as performance can vary substantially across domains and data

distributions.

5. Conclusion

We have introduced LCMem, a cross-domain framework for memorization detection that operates directly in generative latent spaces. By coupling re-identification and copy detection through a single multi-target objective, LCMem consolidates two previously disconnected privacy paradigms into one coherent model. Our experiments across heterogeneous datasets reveal a consistent pattern: existing approaches collapse when confronted with cross-domain variation and lack the robustness needed for reliable privacy auditing. LCMem overcomes these limitations with substantial gains in both tasks, enabling accurate and scalable identification of memorized content in generative

models. These results establish LCMem as a step toward trustworthy and privacy-preserving synthetic data pipelines. Future work will extend toward formal privacy guarantees and deployable protections for real world use cases. Model and code will be released at the conference.

Acknowledgements

HPC resources were provided by the Erlangen National High Performance Computing Center (NHR@FAU), under the NHR projects b143dc and b180dc. NHR is funded by federal and Bavarian state authorities, and NHR@FAU hardware is partially funded by the DFG - 440719683. We acknowledge the use of Isambard-AI National AI Research Resource (AIRR) [43]. Isambard-AI is operated by the University of Bristol and is funded by the UK Government's DSIT via UKRI; and the Science and Technology Facilities Council [ST/AIRR/I-A-I/1023]. The authors received funding from the ERC-project MIA-NORMAL 101083647, DFG 513220538, 512819079, and by the state of Bavaria (HTA).

References

- [1] Rebecca Asiimwe, Stephanie Lam, Samuel Leung, Shanzhao Wang, Rachel Wan, Anna Tinker, Jessica N. McAlpine, Michelle M. M. Woo, David G. Huntsman, and Aline Talhouk. From biobank and data silos into a data commons: convergence to support translational medicine. *Journal of Translational Medicine*, 19:493, 2021. [1](#)
- [2] Alexei Baevski, Wei-Ning Hsu, Qiantong Xu, Arun Babu, Jitao Gu, and Michael Auli. data2vec: A General Framework for Self-supervised Learning in Speech, Vision and Language. In *Proceedings of the 39th International Conference on Machine Learning*, pages 1298–1312. PMLR, 2022. ISSN: 2640-3498. [5, 6](#)
- [3] Mohammed Baharoon, Luyang Luo, Michael Moritz, Abhinav Kumar, Sung Eun Kim, Xiaoman Zhang, Miao Zhu, Mahmoud Hussain Alabbad, Maha Sbayel Alhazmi, Neel P. Mistry, Kent Ryan Kleinschmidt, Brady Chrisler, Sathvik Suryadevara, Sri Sai Dinesh Jaliparthi, Noah Michael Prudlo, Mark David Marino, Jeremy Palacio, Rithvik Akula, Hong-Yu Zhou, Ibrahim Ethem Hamamci, Scott J. Adams, Hassan Rayhan AlOmaish, and Pranav Rajpurkar. ReX-GroundingCT: A 3D Chest CT Dataset for Segmentation of Findings from Free-Text Reports, 2025. arXiv:2507.22030 [eess]. [13](#)
- [4] Hritik Bansal, Da Yin, Masoud Monajatipoor, and Kai-Wei Chang. How well can Text-to-Image Generative Models understand Ethical Natural Language Interventions?, 2022. arXiv:2210.15230 [cs]. [2](#)
- [5] Keith Bonawitz, Hubert Eichner, Wolfgang Grieskamp, Dzmitry Huba, Alex Ingerman, Vladimir Ivanov, Chloe Kiddon, Jakub Konečný, Stefano Mazzocchi, Brendan McMahan, et al. Towards federated learning at scale: System design. *Proceedings of machine learning and systems*, 1:374–388, 2019. [2](#)
- [6] Adam Buick. Copyright and AI training data—transparency to the rescue? *Journal of Intellectual Property Law and Practice*, 20(3):182–192, 2025. [1](#)
- [7] Nicholas Carlini, Steve Chien, Milad Nasr, Shuang Song, Andreas Terzis, and Florian Tramèr. Membership Inference Attacks From First Principles. In *2022 IEEE Symposium on Security and Privacy (SP)*, pages 1897–1914, 2022. ISSN: 2375-1207. [2](#)
- [8] Nicholas Carlini, Jamie Hayes, Milad Nasr, Matthew Jagielinski, Vikash Sehwag, Florian Tramèr, Borja Balle, Daphne Ippolito, and Eric Wallace. Extracting Training Data from Diffusion Models, 2023. arXiv:2301.13188 [cs]. [2](#)
- [9] Mathilde Caron, Ishan Misra, Julien Mairal, Priya Goyal, Piotr Bojanowski, and Armand Joulin. Unsupervised Learning of Visual Features by Contrasting Cluster Assignments. In *NeurIPS*, 2020. [5, 6](#)
- [10] Ting Chen, Simon Kornblith, Mohammad Norouzi, and Geoffrey Hinton. A Simple Framework for Contrastive Learning of Visual Representations, 2020. arXiv:2002.05709 [cs]. [3](#)
- [11] Salman Ul Hassan Dar, Arman Ghanaat, Jannik Kahmann, Isabelle Ayx, Theano Papavassiliu, Stefan O. Schoenberg, and Sandy Engelhardt. Investigating Data Memorization in 3D Latent Diffusion Models for Medical Image Synthesis, 2023. arXiv:2307.01148 [cs, eess]. [2](#)
- [12] Salman Ul Hassan Dar, Marvin Seyfarth, Isabelle Ayx, Theano Papavassiliu, Stefan O. Schoenberg, Robert Malte Stepmann, Fabian Christopher Laqua, Jannik Kahmann, Norbert Frey, Bettina Baeßler, Sebastian Foersch, Daniel Truhn, Jakob Nikolas Kather, and Sandy Engelhardt. Unconditional Latent Diffusion Models Memorize Patient Imaging Data: Implications for Openly Sharing Synthetic Data, 2025. arXiv:2402.01054 [eess]. [2, 3, 5, 6](#)
- [13] Mischa Dombrowski and Bernhard Kainz. Enabling PSO-Secure Synthetic Data Sharing Using Diversity-Aware Diffusion Models, 2025. arXiv:2506.17975 [cs]. [1, 2, 3](#)
- [14] Mischa Dombrowski, Weitong Zhang, Sarah Cechnicka, Hadrien Reynaud, and Bernhard Kainz. Image Generation Diversity Issues and How to Tame Them, 2024. arXiv:2411.16171 [cs]. [2, 4, 5](#)
- [15] Marawan Elbatel, Konstantinos Kamnitsas, and Xiaomeng Li. An Organism Starts with a Single Pix-Cell: A Neural Cellular Diffusion for High-Resolution Image Synthesis, 2024. arXiv:2407.03018 [cs]. [2](#)
- [16] Yannik Frisch, Moritz Fuchs, Antoine Sanner, Felix Anton Ucar, Marius Frenzel, Joana Wasielica-Poslednik, Adrian Gericke, Felix Mathias Wagner, Thomas Dratsch, and Anirban Mukhopadhyay. Synthesising Rare Cataract Surgery Samples with Guided Diffusion Models, 2023. arXiv:2308.02587 [eess]. [3](#)
- [17] Jonas Geiping, Hartmut Bauermeister, Hannah Dröge, and Michael Moeller. Inverting Gradients - How easy is it to break privacy in federated learning? In *Advances in Neural Information Processing Systems*, pages 16937–16947. Curran Associates, Inc., 2020. [2](#)
- [18] Jean-Bastien Grill, Florian Strub, Florent Altché, Corentin Tallec, Pierre H. Richemond, Elena Buchatskaya, Carl Do-

ersch, Bernardo Avila Pires, Zhaohan Daniel Guo, Mhammad Gheshlaghi Azar, Bilal Piot, Koray Kavukcuoglu, Rémi Munos, and Michal Valko. Bootstrap your own latent: A new approach to self-supervised Learning, 2020. arXiv:2006.07733 [cs, stat]. 5, 6

[19] Hao Guan, Pew-Thian Yap, Andrea Bozoki, and Mingxiao Liu. Federated learning for medical image analysis: A survey. *Pattern Recognition*, 151:110424, 2024. 1, 2

[20] Ibrahim Ethem Hamamci, Sezgin Er, Chenyu Wang, Furkan Almas, Ayse Gulnihan Simsek, Seval Nil Esirgun, Irem Doga, Omer Faruk Durugol, Weicheng Dai, Murong Xu, Muhammed Furkan Dasdelen, Bastian Wittmann, Tamaz Amiranashvili, Enis Simsar, Mehmet Simsar, Emine Bensu Erdemir, Abdullah Alanbay, Anjany Sekuboyina, Berkana Lafci, Christian Blauthgen, Kayhan Batmanghelich, Mehmet Kemal Ozdemir, and Bjoern Menze. Developing Generalist Foundation Models from a Multimodal Dataset for 3D Computed Tomography, 2025. arXiv:2403.17834 [cs]. 5

[21] Kun Han, Yifeng Xiong, Chenyu You, Pooya Khosravi, Shanlin Sun, Xiangyi Yan, James Duncan, and Xiaohui Xie. MedGen3D: A Deep Generative Framework for Paired 3D Image and Mask Generation, 2023. arXiv:2304.04106 [eess]. 3

[22] Kaiming He, Xinlei Chen, Saining Xie, Yanghao Li, Piotr Dollar, and Ross Girshick. Masked Autoencoders Are Scalable Vision Learners. In *2022 IEEE/CVF Conference on Computer Vision and Pattern Recognition (CVPR)*, pages 15979–15988, New Orleans, LA, USA, 2022. IEEE. 5, 6

[23] Jonathan Ho and Tim Salimans. Classifier-Free Diffusion Guidance, 2022. arXiv:2207.12598. 2

[24] Jonathan Ho, Ajay Jain, and Pieter Abbeel. Denoising diffusion probabilistic models. *Advances in neural information processing systems*, 33:6840–6851, 2020. 2

[25] Gregory Holste, Song Wang, Ziyu Jiang, Thomas C. Shen, George Shih, Ronald M. Summers, Yifan Peng, and Zhangyang Wang. Long-Tailed Classification of Thorax Diseases on Chest X-Ray: A New Benchmark Study. In *Data Augmentation, Labelling, and Imperfections*, pages 22–32. Springer Nature Switzerland, Cham, 2022. Series Title: Lecture Notes in Computer Science. 5

[26] Zeyi Hou, Ruixin Yan, Qizheng Wang, Ning Lang, and Xizhuang Zhou. Diversity-preserving chest radiographs generation from reports in one stage. In *International Conference on Medical Image Computing and Computer-Assisted Intervention*, pages 482–492. Springer, 2023. 3

[27] Kun Huang, Xiao Ma, Yuhang Zhang, Na Su, Songtao Yuan, Yong Liu, Qiang Chen, and Huazhu Fu. Memory-efficient High-resolution OCT Volume Synthesis with Cascaded Amortized Latent Diffusion Models, 2024. arXiv:2405.16516 [eess]. 3

[28] Alistair E. W. Johnson, Tom J. Pollard, Seth J. Berkowitz, Nathaniel R. Greenbaum, Matthew P. Lungren, Chih Ying Deng, Roger G. Mark, and Steven Horng. MIMIC-CXR, a de-identified publicly available database of chest radiographs with free-text reports. *Scientific Data*, 6(1), 2019. Publisher: Nature Research. 5

[29] Peter Kairouz, H. Brendan McMahan, Brendan Avent, Aurélien Bellet, Mehdi Benni, Arjun Nitin Bhagoji, Kallista Bonawitz, Zachary Charles, Graham Cormode, Rachel Cummings, Rafael G. L. D’Oliveira, Hubert Eichner, Salim El Rouayheb, David Evans, Josh Gardner, Zachary Garrett, Adrià Gascón, Badih Ghazi, Phillip B. Gibbons, Marco Gruteser, Zaid Harchaoui, Chaoyang He, Lie He, Zhouyuan Huo, Ben Hutchinson, Justin Hsu, Martin Jaggi, Tara Javidi, Gauri Joshi, Mikhail Khodak, Jakub Konecný, Aleksandra Korolova, Farinaz Koushanfar, Sanmi Koyejo, Tancrède Lepoint, Yang Liu, Prateek Mittal, Mehryar Mohri, Richard Nock, Ayfer Özgür, Rasmus Pagh, Hang Qi, Daniel Ramage, Ramesh Raskar, Mariana Raykova, Dawn Song, Weikang Song, Sebastian U. Stich, Ziteng Sun, Ananda Theertha Suresh, Florian Tramèr, Praneeth Vepakomma, Jianyu Wang, Li Xiong, Zheng Xu, Qiang Yang, Felix X. Yu, Han Yu, and Sen Zhao. Advances and Open Problems in Federated Learning. *Foundations and Trends® in Machine Learning*, 14(1–2):1–210, 2021. 1

[30] Tero Karras, Miika Aittala, Timo Aila, and Samuli Laine. Elucidating the Design Space of Diffusion-Based Generative Models, 2022. arXiv:2206.00364 [cs]. 2, 3

[31] Tero Karras, Miika Aittala, Tuomas Kynkänniemi, Jaakko Lehtinen, Timo Aila, and Samuli Laine. Guiding a Diffusion Model with a Bad Version of Itself, 2024. arXiv:2406.02507 [cs, stat].

[32] Tero Karras, Miika Aittala, Jaakko Lehtinen, Janne Hellsten, Timo Aila, and Samuli Laine. Analyzing and Improving the Training Dynamics of Diffusion Models, 2024. arXiv:2312.02696 [cs, stat]. 2

[33] Adil Koeken, Alexander Ziller, Moritz Knolle, and Daniel Rueckert. Sensitivity, Specificity, and Consistency: A Tripartite Evaluation of Privacy Filters for Synthetic Data Generation, 2025. arXiv:2510.01793 [cs]. 2

[34] Martin Kretschmer, Thomas Margoni, and Pinar Oruç. Copyright Law and the Lifecycle of Machine Learning Models. *IIC - International Review of Intellectual Property and Competition Law*, 55(1):110–138, 2024. 1

[35] Nicky Kriplani, Minh Pham, Gowthami Somepalli, Chinmay Hegde, and Niv Cohen. SolidMark: Evaluating Image Memorization in Generative Models, 2025. arXiv:2503.00592 [cs]. 2

[36] Guang Li, Ren Togo, Takahiro Ogawa, and Miki Haseyama. Compressed gastric image generation based on soft-label dataset distillation for medical data sharing. *Computer Methods and Programs in Biomedicine*, 227:107189, 2022. 2

[37] Tian Li, Anit Kumar Sahu, Manzil Zaheer, Maziar Sanjabi, Ameet Talwalkar, and Virginia Smith. Federated optimization in heterogeneous networks. *Proceedings of Machine learning and systems*, 2:429–450, 2020. 2

[38] Ziwei Liu, Ping Luo, Xiaogang Wang, and Xiaoou Tang. Deep Learning Face Attributes in the Wild, 2015. arXiv:1411.7766 [cs]. 5

[39] Ziwei Liu, Zhongqi Miao, Xiaohang Zhan, Jiayun Wang, Boqing Gong, and Stella X. Yu. Large-Scale Long-Tailed Recognition in an Open World, 2019. arXiv:1904.05160 [cs] version: 2. 5

[40] Zhuang Liu, Hanzi Mao, Chao-Yuan Wu, Christoph Feichtner, Trevor Darrell, and Saining Xie. A ConvNet for the 2020s, 2022. arXiv:2201.03545. 3, 5, 6

[41] Zeyu Liu, Tianyi Zhang, Yufang He, and Guanglei Zhang. Generating Progressive Images from Pathological Transitions Via Diffusion Model. In *Medical Image Computing and Computer Assisted Intervention – MICCAI 2024*, pages 308–318. Springer Nature Switzerland, Cham, 2024. 2

[42] Thomas Margoni and Martin Kretschmer. A deeper look into the eu text and data mining exceptions: harmonisation, data ownership, and the future of technology. *GRUR international*, 71(8):685–701, 2022. 1

[43] Simon McIntosh-Smith, Sadaf Alam, and Christopher Woods. Isambard-ai: a leadership-class supercomputer optimised specifically for artificial intelligence. In *Proceedings of the Cray User Group*, pages 44–54. 2024. 9

[44] Brendan McMahan, Eider Moore, Daniel Ramage, Seth Hampson, and Blaise Aguera y Arcas. Communication-Efficient Learning of Deep Networks from Decentralized Data. In *Proceedings of the 20th International Conference on Artificial Intelligence and Statistics*, pages 1273–1282. PMLR, 2017. ISSN: 2640-3498. 1

[45] M. Molina and F. Burn. Memorization detection benchmark for generative image models. In *NeurIPS Safe Generative AI Workshop*, 2024. 2

[46] Inye Na, Jonghun Kim, Eun Sook Ko, and Hyunjin Park. RadiomicsFill-Mammo: Synthetic Mammogram Mass Manipulation with Radiomics Features, 2024. 3

[47] Dianwen Ng, Xiang Lan, Melissa Min-Szu Yao, Wing P. Chan, and Mengling Feng. Federated learning: a collaborative effort to achieve better medical imaging models for individual sites that have small labelled datasets. *Quantitative Imaging in Medicine and Surgery*, 11(2):852–857, 2021. 1

[48] Kobbi Nissim. Privacy: From Database Reconstruction to Legal Theorems. In *Proceedings of the 40th ACM SIGMOD-SIGACT-SIGAI Symposium on Principles of Database Systems*, pages 33–41, Virtual Event China, 2021. ACM. 1

[49] Jamie A. O'Reilly and Fawad Asadi. Pre-trained vs. Random Weights for Calculating Fréchet Inception Distance in Medical Imaging. In *2021 13th Biomedical Engineering International Conference (BMEiCON)*, pages 1–4, Ayutthaya, Thailand, 2021. IEEE. 5, 6

[50] Hyun-Jic Oh and Won-Ki Jeong. Controllable and Efficient Multi-Class Pathology Nuclei Data Augmentation using Text-Conditioned Diffusion Models, 2024. arXiv:2407.14426 [cs]. 2

[51] Maxime Oquab, Timothée Darcet, Théo Moutakanni, Huy Vo, Marc Szafraniec, Vasil Khalidov, Pierre Fernandez, Daniel Haziza, Francisco Massa, Alaaeldin El-Nouby, Mahmoud Assran, Nicolas Ballas, Wojciech Galuba, Russell Howes, Po-Yao Huang, Shang-Wen Li, Ishan Misra, Michael Rabbat, Vasu Sharma, Gabriel Synnaeve, Hu Xu, Hervé Jegou, Julien Mairal, Patrick Labatut, Armand Joulin, and Piotr Bojanowski. DINoV2: Learning Robust Visual Features without Supervision, 2024. arXiv:2304.07193 [cs]. 5, 6

[52] Kai Packhäuser, Sebastian Gündel, Nicolas Münster, Christopher Syben, Vincent Christlein, and Andreas Maier. Deep learning-based patient re-identification is able to exploit the biometric nature of medical chest X-ray data. *Scientific Reports*, 12(1):14851, 2022. 2, 3, 5, 6

[53] Alec Radford, Jong Wook Kim, Chris Hallacy, Aditya Ramesh, Gabriel Goh, Sandhini Agarwal, Girish Sastry, Amanda Askell, Pamela Mishkin, Jack Clark, Gretchen Krueger, and Ilya Sutskever. Learning Transferable Visual Models From Natural Language Supervision, 2021. arXiv:2103.00020. 5, 6

[54] Jie Ren, Yixin Li, Shenglai Zeng, Han Xu, Lingjuan Lyu, Yue Xing, and Jiliang Tang. Unveiling and Mitigating Memorization in Text-to-image Diffusion Models through Cross Attention, 2024. arXiv:2403.11052 [cs]. 2

[55] Hadrien Reynaud, Qingjie Meng, Mischa Dombrowski, Arjit Ghosh, Thomas Day, Alberto Gomez, Paul Leeson, and Bernhard Kainz. EchoNet-Synthetic: Privacy-preserving Video Generation for Safe Medical Data Sharing, 2024. arXiv:2406.00808 [cs]. 2, 3

[56] Nicola Rieke, Jonny Hancox, Wenqi Li, Fausto Milletari, Holger R. Roth, Shadi Albarqouni, Spyridon Bakas, Mathieu N. Galtier, Bennett A. Landman, Klaus Maier-Hein, Sébastien Ourselin, Micah Sheller, Ronald M. Summers, Andrew Trask, Daguang Xu, Maximilian Baust, and M. Jorge Cardoso. The future of digital health with federated learning. *npj Digital Medicine*, 3(1):119, 2020. 1

[57] Robin Rombach, Andreas Blattmann, Dominik Lorenz, Patrick Esser, and Björn Ommer. High-Resolution Image Synthesis with Latent Diffusion Models, 2022. arXiv:2112.10752 [cs]. 2, 3

[58] Veronica Rotemberg, Nicholas Kurtansky, Brigid Betz-Stablein, Liam Caffery, Emmanouil Chousakos, Noel Codella, Marc Combalia, Stephen Dusza, Pascale Guitera, David Gutman, Allan Halpern, Brian Helba, Harald Kittler, Kivanc Kose, Steve Langer, Konstantinos Lioprys, Josep Malvehy, Shenara Musthaq, Jabpani Nanda, Ofer Reiter, George Shih, Alexander Stratigos, Philipp Tschandl, Jochen Weber, and H. Peter Soyer. A patient-centric dataset of images and metadata for identifying melanomas using clinical context. *Scientific Data*, 8(1):34, 2021. 5

[59] Mohammad Ali Saberi, Hamid Mcheick, and Mehdi Adda. From Data Silos to Health Records Without Borders: A Systematic Survey on Patient-Centered Data Interoperability. *Information*, 16(2):106, 2025. 1

[60] Oriane Siméoni, Huy V. Vo, Maximilian Seitzer, Federico Baldassarre, Maxime Oquab, Cijo Jose, Vasil Khalidov, Marc Szafraniec, Seungeun Yi, Michaël Ramamonjisoa, Francisco Massa, Daniel Haziza, Luca Wehrstedt, Jianyuan Wang, Timothée Darcet, Théo Moutakanni, Leonel Sentana, Claire Roberts, Andrea Vedaldi, Jamie Tolan, John Brandt, Camille Couprie, Julien Mairal, Hervé Jégou, Patrick Labatut, and Piotr Bojanowski. DINoV3, 2025. 5, 6

[61] Jiaming Song, Chenlin Meng, and Stefano Ermon. Denoising Diffusion Implicit Models, 2022. arXiv:2010.02502 [cs]. 2

[62] George Stein, Jesse C. Cresswell, Rasa Hosseinzadeh, Yi Sui, Brendan Leigh Ross, Valentin Villecroze, Zhaoyan Liu, Anthony L. Caterini, J. Eric T. Taylor, and Gabriel Loaiza-

Ganem. Exposing flaws of generative model evaluation metrics and their unfair treatment of diffusion models, 2023. arXiv:2306.04675 [cs, stat]. 5

[63] Christian Szegedy, Vincent Vanhoucke, Sergey Ioffe, Jon Shlens, and Zbigniew Wojna. Rethinking the Inception Architecture for Computer Vision. In *2016 IEEE Conference on Computer Vision and Pattern Recognition (CVPR)*, pages 2818–2826, Las Vegas, NV, USA, 2016. IEEE. 5, 6

[64] Nicholas Vollmer. Recital 26 EU General Data Protection Regulation (EU-GDPR), 2023. Publisher: SecureDataService. 1

[65] Fan Wang, Zehua Ren, Chunfeng Lian, and Jianhua Ma. Controllable Counterfactual Generation for Interpretable Medical Image Classification. In *Medical Image Computing and Computer Assisted Intervention – MICCAI 2024*, pages 143–152. Springer Nature Switzerland, Cham, 2024. Series Title: Lecture Notes in Computer Science. 2

[66] Xiaosong Wang, Yifan Peng, Le Lu, Zhiyong Lu, Mohammad Bagheri, and Ronald M Summers. Chestx-ray8: Hospital-scale chest x-ray database and benchmarks on weakly-supervised classification and localization of common thorax diseases. In *Proceedings of the IEEE conference on computer vision and pattern recognition*, pages 2097–2106, 2017. 5

[67] Zhou Wang, A.C. Bovik, H.R. Sheikh, and E.P. Simoncelli. Image quality assessment: from error visibility to structural similarity. *IEEE Transactions on Image Processing*, 13(4): 600–612, 2004. 5

[68] Max Welling. Herding dynamical weights to learn. In *Proceedings of the 26th Annual International Conference on Machine Learning*, pages 1121–1128, Montreal Quebec Canada, 2009. ACM. 2

[69] Tonya White, Elisabet Blok, and Vince D. Calhoun. Data sharing and privacy issues in neuroimaging research: Opportunities, obstacles, challenges, and monsters under the bed. *Human Brain Mapping*, 43(1):278–291, 2020. 1

[70] Mohammed Elbachir Yahiaoui, Makhlof Derdour, Rawad Abdulghafor, Sherzod Turaev, Mohamed Gasmi, Akram Bennour, Abdulaziz Aborujilah, and Mohamed Al Sarem. Federated Learning with Privacy Preserving for Multi- Institutional Three-Dimensional Brain Tumor Segmentation. *Diagnostics*, 14(24):2891, 2024. 1

[71] Ling Yang, Zhilong Zhang, Yang Song, Shenda Hong, Runsheng Xu, Yue Zhao, Wentao Zhang, Bin Cui, and Ming-Hsuan Yang. Diffusion models: A comprehensive survey of methods and applications. *ACM computing surveys*, 56(4): 1–39, 2023. 2

[72] Ruonan Yu, Songhua Liu, and Xinchao Wang. Dataset Distillation: A Comprehensive Review, 2023. arXiv:2301.07014 [cs]. 2

[73] Zhouhang Yuan, Zhengqing Fang, Zhengxing Huang, Fei Wu, Yu-Feng Yao, and Yingming Li. Adapting Pre-trained Generative Model to Medical Image for Data Augmentation. In *Medical Image Computing and Computer Assisted Intervention – MICCAI 2024*, pages 79–89. Springer Nature Switzerland, Cham, 2024. Series Title: Lecture Notes in Computer Science. 2

[74] Yunpeng Zhao and Jie Zhang. Does training with synthetic data truly protect privacy? *arXiv preprint arXiv:2502.12976*, 2025. 2, 7

[75] Zhekai Zhou, Guibo Luo, Mingzhi Chen, Zhenyu Weng, and Yuesheng Zhu. Federated Learning for Medical Image Classification: A Comprehensive Benchmark, 2025. arXiv:2504.05238 [cs]. 2

[76] Ligeng Zhu, Zhijian Liu, and Song Han. Deep Leakage from Gradients. In *Advances in Neural Information Processing Systems*. Curran Associates, Inc., 2019. 2

[77] Alexander Ziller, Tamara T. Mueller, Simon Stieger, Leonhard F. Feiner, Johannes Brandt, Rickmer Braren, Daniel Rueckert, and Georgios Kaassis. Reconciling privacy and accuracy in AI for medical imaging. *Nature Machine Intelligence*, 6(7):764–774, 2024. 2

A. Dataset Preprocessing

The CTRate dataset consists of volumetric chest CT scans. To enable training on two-dimensional images, we extract 2D slices that contain clinically described findings. Using RexGrounding-CT annotations from Baharoon et al. [3], we identify and retain slices that either include or exclude abnormal findings. For each finding instance, we extract all corresponding segmentation masks and include one representative image slice per instance in the final dataset. To maintain balance, we also add a single slice without any labeled findings for each abnormal slice. Note that such “negative” slices are not guaranteed to be healthy, as the labeling process in RexGrounding-CT is not exhaustive [3]. Each slice receives multi-label annotations according to the segmentation masks, allowing multiple co-occurring diseases to be captured.

B. LCMem Training Details

LCMem is trained in two stages. In the first stage the model is optimized entirely in the latent space of the Stable Diffusion 2 VAE. All training images are encoded once into four channel latent tensors of resolution 64×64 , which are then used throughout the latent pretraining phase. The goal of this stage is to learn a stable similarity representation of the two input images that reflects the structure encoded in the latent space. To achieve this, augmentation is intentionally minimal and only introduces a very small probability of channel wise normalization, while rotations, flips, blur, and noise are disabled. The model is trained with a batch size of 512 and a learning rate of $5 \cdot 10^{-4}$ until convergence.

In the second stage the network is fine tuned on image data but still operates on VAE encoded latents. Each image is first augmented in pixel space and is then passed through the frozen Stable Diffusion 2 VAE before being processed by the network. This stage uses a stronger augmentation regime that applies rotations up to 20° , horizontal flips, Gaussian blur, additive noise, brightness and contrast jitter, and JPEG compression with quality between 10 and 95. The learning rate is reduced to $8 \cdot 10^{-5}$ and the batch size to 64. This procedure allows the model to retain the structure learned in latent space while becoming robust to realistic perturbations in clinical imaging workflows, resulting in a coherent embedding space used for all experiments in the main paper.